Supplementary Information

Three-Dimensional Flexible Electrode Derived from Low-Cost Nickel-Phytate with Improved Electrochemical Performance

Panpan Li, [a, b] Zhaoyu Jin, [b] Rui Wang,[c] Yong Jin[c, *], Dan Xiao[b, *]

Table S1. Composition and operating conditions of the coating baths for depositing nickel.

$NiSO_4 \cdot 6H_2O$ (g L^{-1})	28
$NaH_2PO_2 \cdot H_2O$ (g L^{-1})	20
$NaC_2H_3O_2$ (g L^{-1})	5
Tri-sodium citrate (g L^{-1})	5
pH	4 ~ 5
Temperature (°C)	80 ~ 90

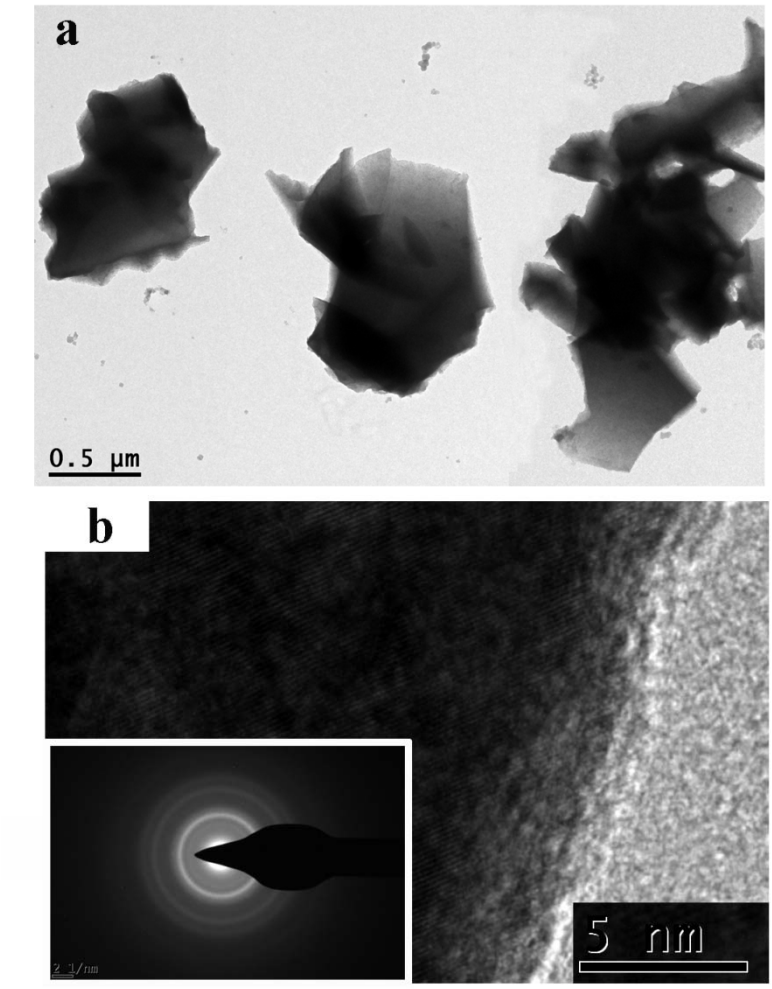

Fig. S1 The TEM images of Ni-phytate nanoplates and the corresponding SAED in panel b.

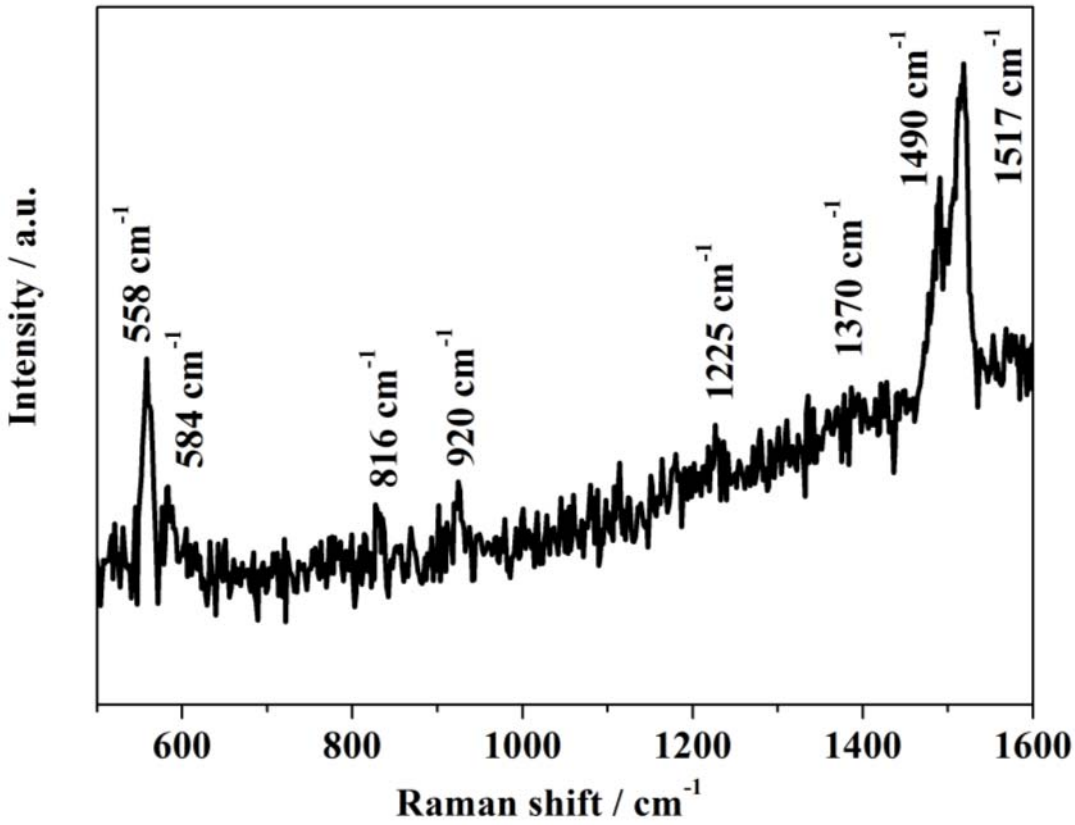

Fig. S2 The Raman pattern of 3D-NA/Ni/NiNPAs.

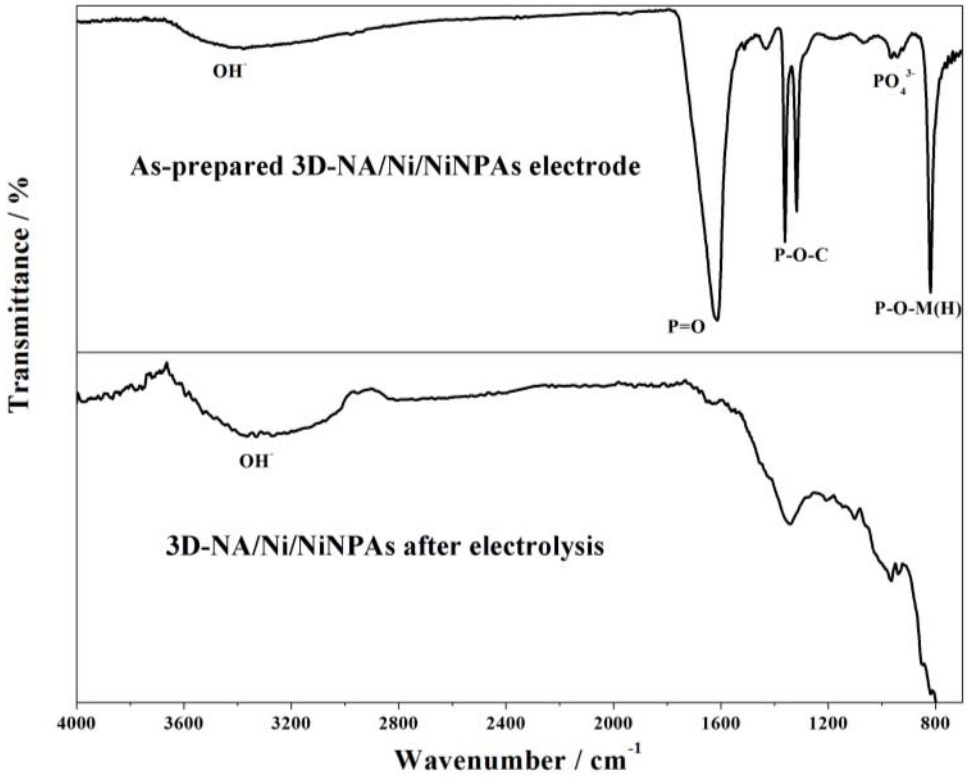

Fig. S3 The ATR-IR spectra of 3D-NA/Ni/NiNPAs before and after electrolysis.

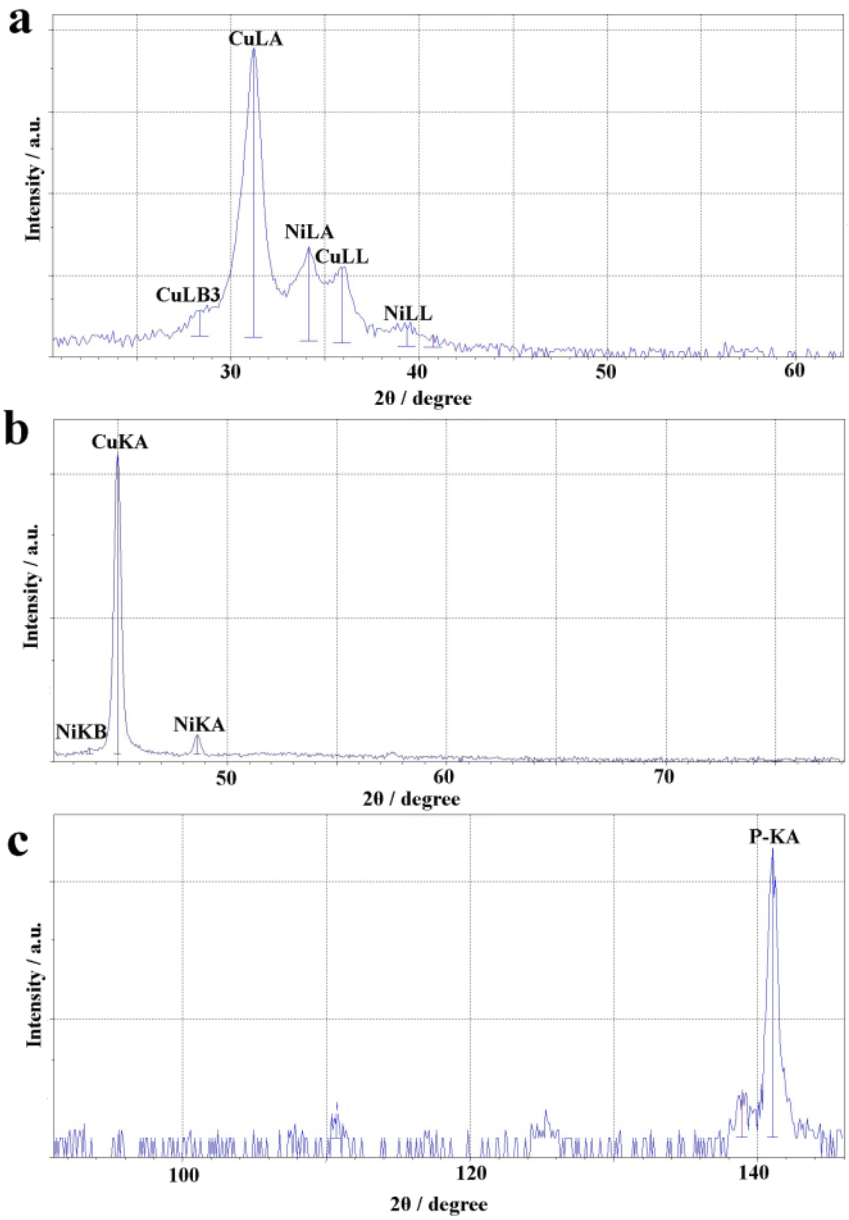

Fig. S4 XRF spectra of PL/Ni substrate at different diffraction degrees.

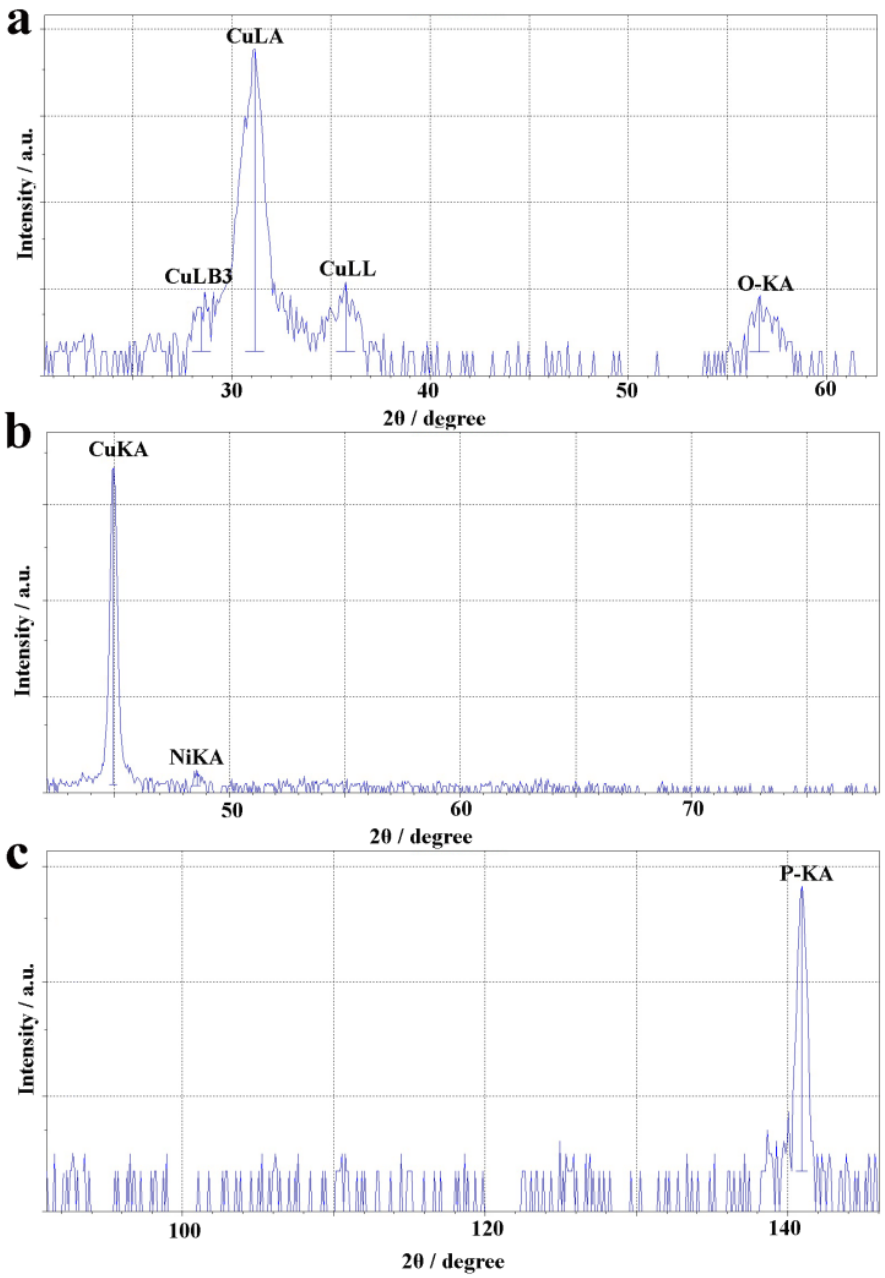

Fig. S5 XRF spectra of PL/Ni/NiNPAs substrate at different diffraction degrees.

Table S2. The quantitative analysis of elements on the surface of PL-Ni and PL-NiNPAs.

PL/Ni		**PL/Ni/NiNPAs**	
E[a]	**C**[b] **/ %**	**E**	**C / %**
P	0.553	P	1.053
Ni	17.543	Ni	0.175
Cu	81.905	Cu	60.959
O	—	O	37.813

[a]E: the abbreviation of elements. [b]C: the abbreviation of concentration.

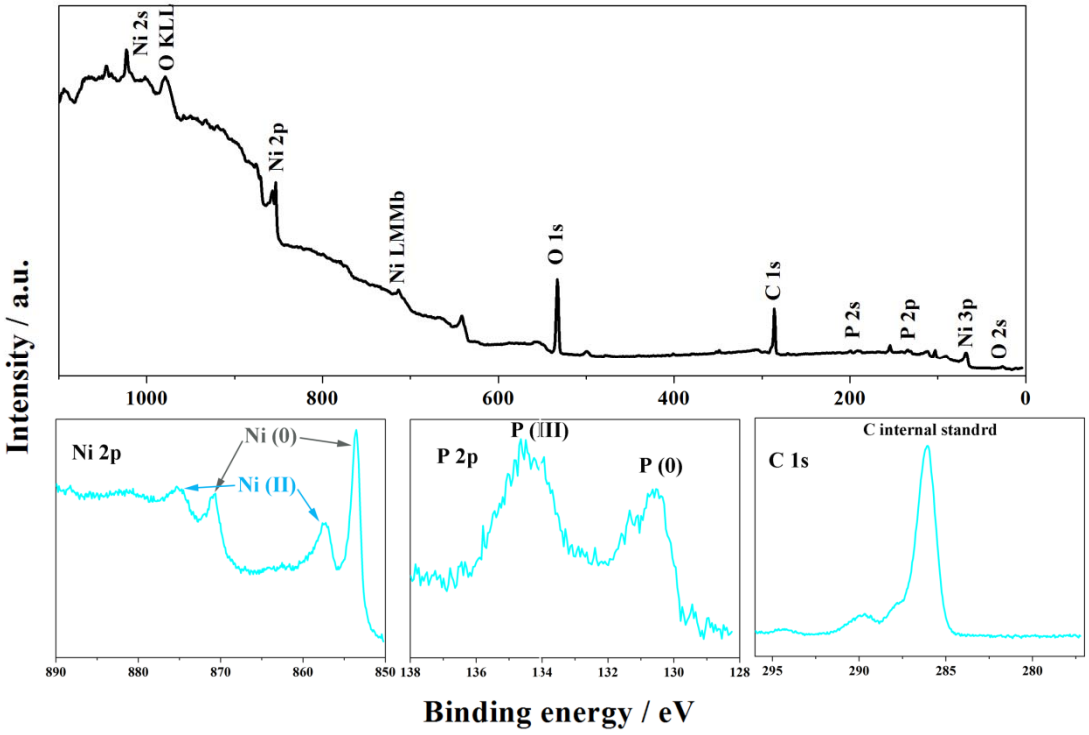

Fig. S6 The survey scan XPS spectra and of 3D-NA/Ni substrate.

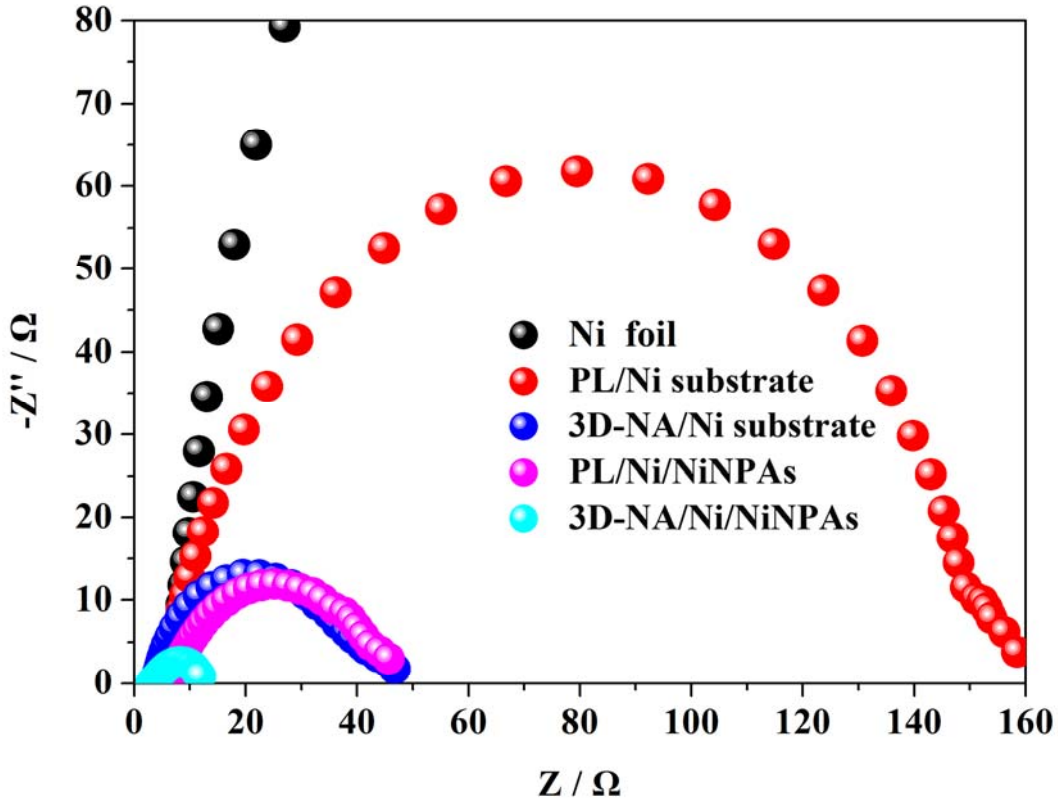

Fig. S7 EIS of several electrodes at the applied potential of ~1.57 V vs. RHE.

Table S3. The value of electron transfer resistance (R_{ct}) for various electrodes in the of Fig. S7 based on the equivalent circuit diagram below.

Work electrodes	R_{ct} / Ω
Commercial Ni foil	2218
PL/Ni substrate	165.1
3D-NA substrate	32.65
PL/Ni/NiNiNPAs	39.55
3D-NA/Ni/NiNPAs	11.68

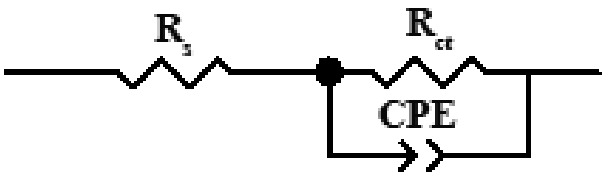

* The corresponding equivalent circuit diagram consisting of a R_s, a R_{ct}, and a constant-phase element (CPE).

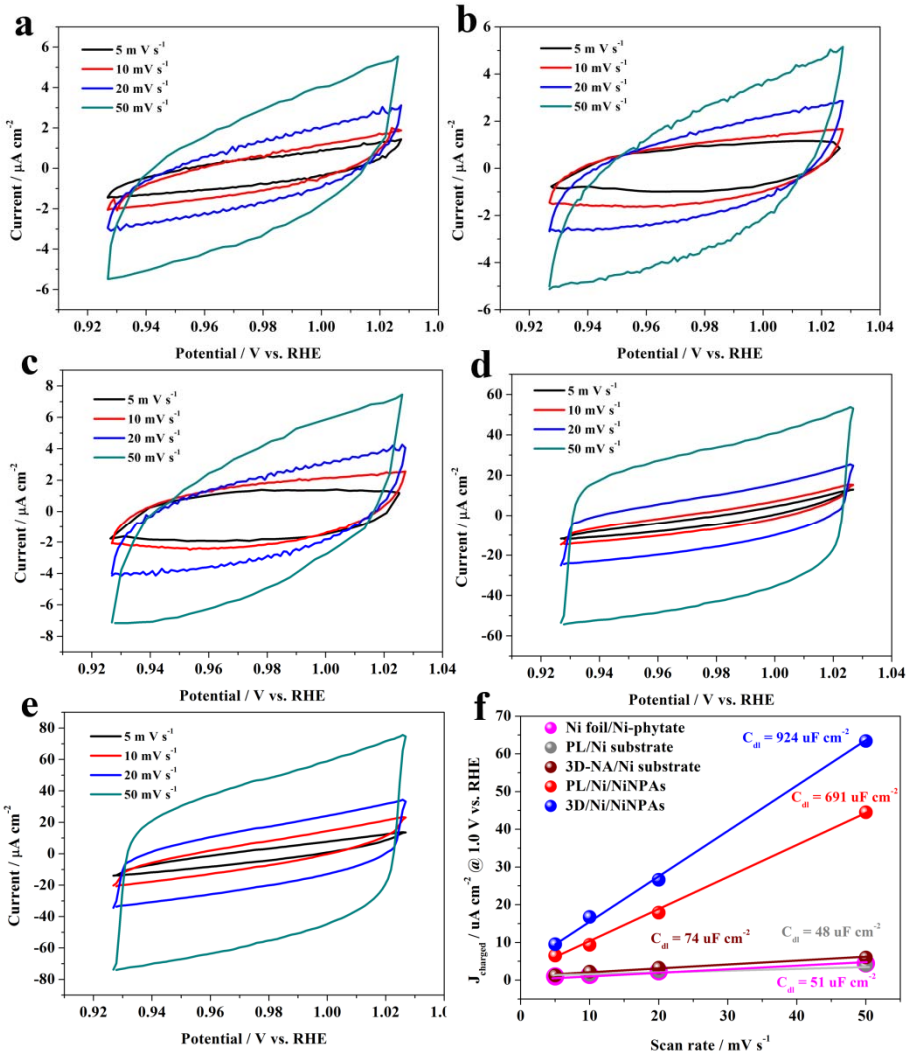

Fig. S8 Electrochemical double-layer capacitance measurements of Ni foil/Ni-phytate (a), PL/Ni substrate (b), 3D-NA/Co substrate (c), PL/Ni/NiNPAs (d) and 3D-NA/Ni/NiNPAs (e) at the scan rates of 5, 10, 20 and 50 mV s^{-1} in 1 M KOH; (f) linear fitting curves of the oxidation currents at 1.0 V (vs. RHE) of each electrode vs. scan rates.

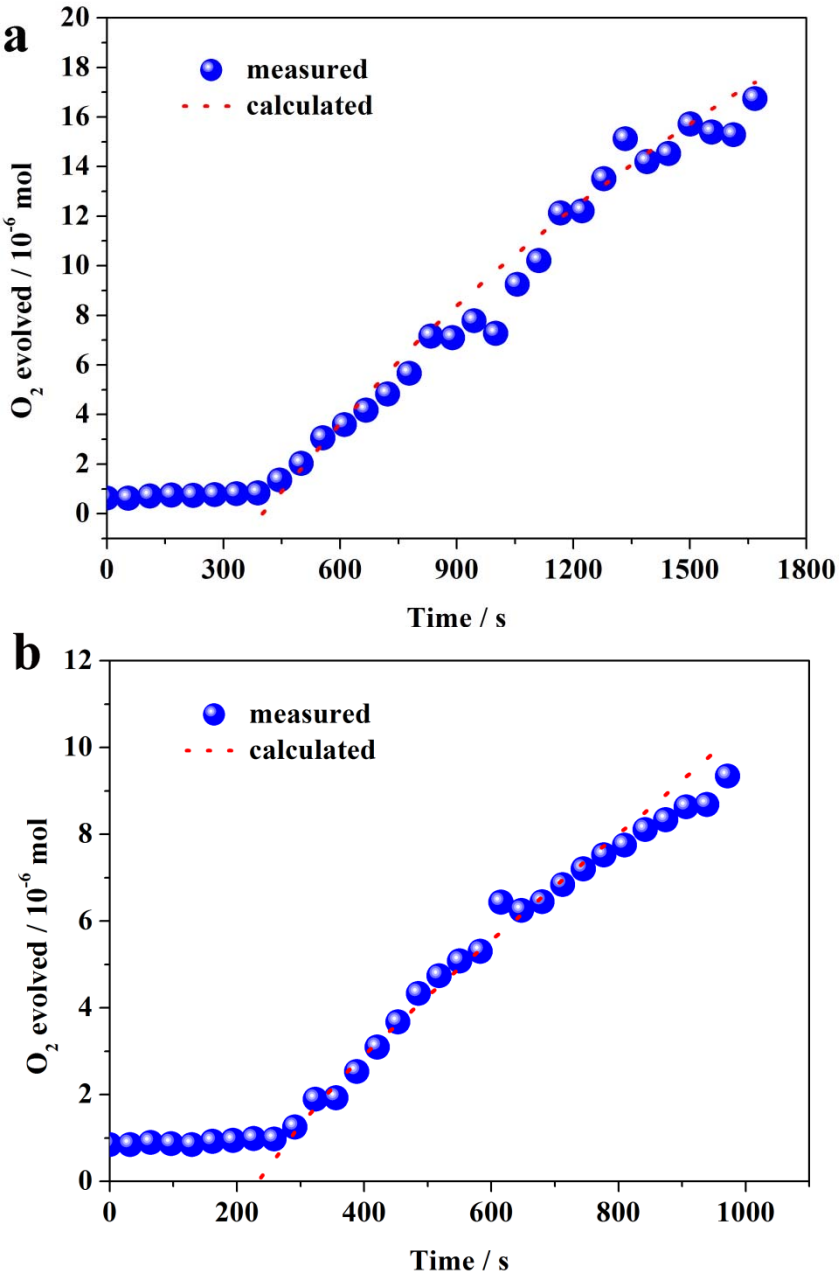

Fig. S9 The Faradic efficiency testing of PL/Ni/NiNPAs (a) and 3D-NA/Ni/NiNPAs (b) in 1 M KOH. The spots are the actual oxygen production that obtained via PASCO oxygen sensor (USA) along with the Henry's law at a stable current of 4.8 mA for PL/Ni/NiNPAs and 5.5 mA for 3D-NA/ Ni/NiNPAs; the dot lines are the theoretical values.

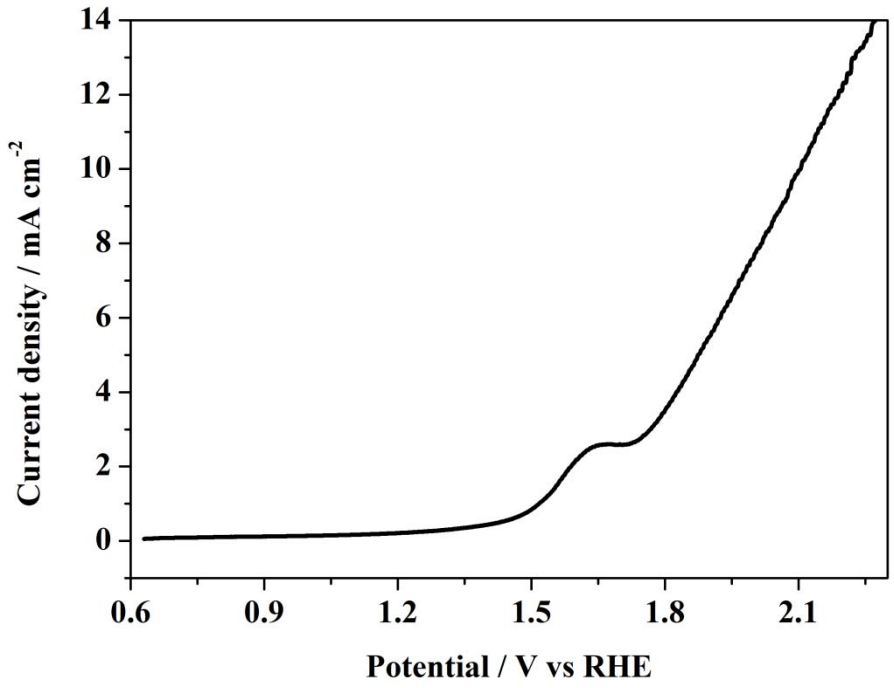

Fig. S10 LSV measurement of 3D-NA/Ni/NiNPAs electrode with the scan rate of 5 mV s^{-1} in 0.2 M borate buffer solution (pH = 9.2).

Table S4 Comparison of OER performances of Ni-based electrocatalyst.

Electrode and Experimental condition	**Geometrical surface area and mass loading**	**Onset Potential[a]/mV**	**η^{b} @ 10 mA cm^{-2} / mV**	**J @ η = 0.32 V mA cm^{-2}**	**Stability**	**Ref.**
$Ni_{0.9}Fe_{0.1}$/NC on glassy carbon, 1 M KOH	0.196 cm^2, 0.2 mg cm^{-2}	~ 270	330	~ 5	An increase of 25 mV after 10000 cycles at 10 mA cm^{-2}	[1]
MWCNTs/$Ni(OH)_2$ on ITO, 0.1 M KOH	0.28 mg cm^{-2}	322	474	~ 1	100 % current density retention after 6 hours' electrocatalysis at η = 0.435 V	[2]
FeNi@NC on glassy carbon, 1 M KOH	0.196 cm^2, 0.32 mg cm^{-2}	210	280	20	A slight increase in potential after 10000 cycles at 100 mA cm^{-2} and 40 mA cm^{-2}	[3]
$Li_{1.03}Ni0.66Co_{0.21}Fe_{0.10}O_{1.95}$ on glassy carbon, 0.1 M KOH	0.196 cm^2, 0.128 mg cm^{-2}	283	375	~ 1	Onset potential remains the same after 60 minutes' electrocatalysis at 10 mA cm^{-2}	[4]
α-Ni(OH)2 spheres on glassy carbon, 0.1 M KOH	0.196 cm^2, 0.2 mg cm^{-2}	-	331	< 10	> 100 % current density retention after 330 minutes' electrocatalysis at η = 340 mV	[5]
Ni_3S_2 Nanosheet grown on Ni foam, 1 M NaOH	0.09 cm^2, 1.6 mg cm^{-2}	~ 120	260	~ 25	~ 100 % current density retention after 200 hours' electrocatalysis at η = 260 mV	[6]
CoNi(OH)x grown on Cu film, 1 M KOH	0.72 mg cm^{-2}	250	280	~63	64% current density retention after 24 hours' electrocatalysis at η = 320 mV	[7]
NiCo-LDH grown on carbon paper, 1 M KOH	0.17 mg cm^{-2}	-	367	~2	An increase of 22 mV after 6 hours' electrocatalysis at 10 mA cm^{-2}	[8]
Ni NPs in N-doped graphene films, 0.1 M KOH	0.91 mg cm^{-2}	-	~ 340	~ 8	> 100 % current density retention after 12 hours' electrocatalysis at η = 440 mV	[9]
Ni–Co oxide-HNSs grown on FTO, 1.0 M NaOH	0.25 cm^2	290	340	5	96 % current density retention after 18 hours' electrocatalysis at η = 370 mV	[10]

$NiCo_2O_4$ nanowires grown on Ti foil, 1 M KOH	0.3 mg cm^{-2}	330	370	~0	~ 93% current density retention after 20 hours' electrocatalysis at η = 420 mV	[11]
Fe_6Ni_{10} on glassy carbon, 1 M KOH	0.072 cm^2, 0.10 mg cm^{-2}	-	286	20	-	[12]
NiFe-NS on glassy carbon, 1 M KOH	0.071 cm^2, 0.07 mg cm^{-2}	260	302	25	An increase of 20 mV in potential after 6 hours' electrocatalysis at 10 mA cm^{-2}	[13]
Ni_2P on glassy carbon, 1 M KOH	0.071 cm^2, 0.14 mg cm^{-2}	-	290	~20	An increase of 10 mV after 10 hours' electrocatalysis at 10 mA cm^{-2}	[14]
3D-NA/Ni/NiNPAs grown on Cu-coated polyimide film, 1 M KOH	0.25 cm^2, 0.3 mg cm^{-2}	220	285	25	94 % current density retention after 175 hours' electrocatalysis at η = 340 mV	This work
3D-NA/RuO_2 on Cu-coated polyimide film, 1 M KOH	0.25 cm^2, 0.28 mg cm^{-2}	210	310	13	-	This work

[a]the potential at which the reaction occurred; [b] η infers to overprotential.

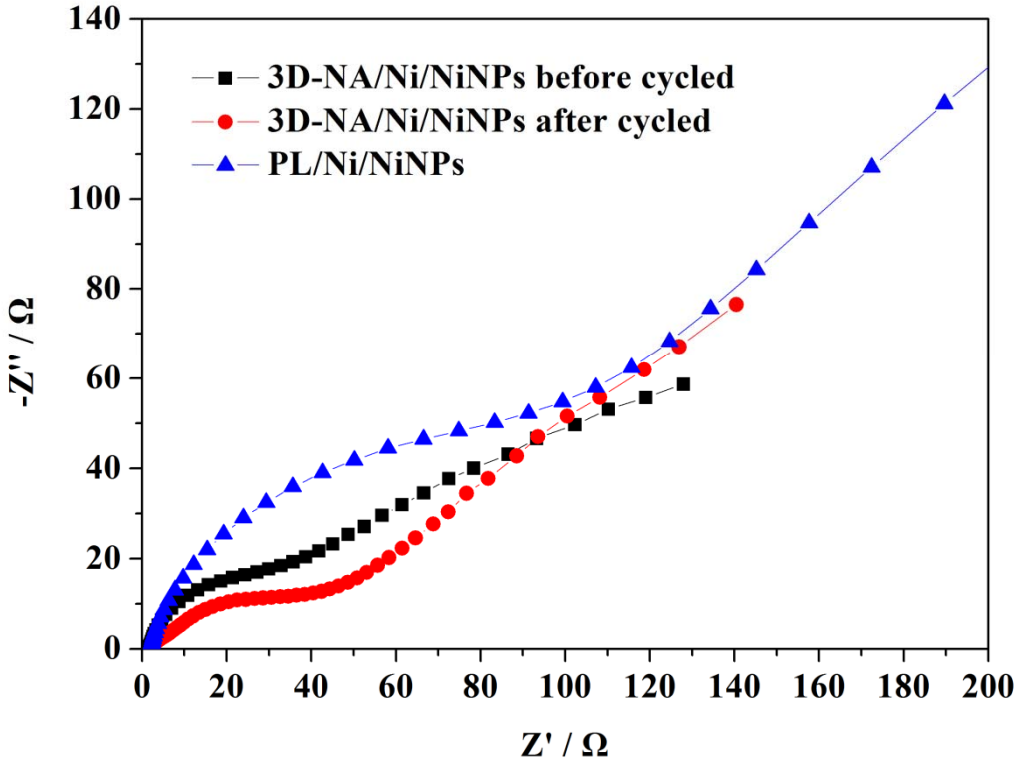

Fig. S11 EIS of 3D-NA/Ni/NiNPAs before and after cycled as well as PL/Ni/NiNPAs electrodes at the open circuit potential.

Table S5 Comparison of capacitance performances of Ni-based materials.

Substrate	Materials	Specific capacitance at 2 mA cm^{-2}	Mass loading	Cycling performance	Ref.
Ni foam	**Ni-CNTs@β-Ni($OH)_2$**	1283 F g^{-1}	1-2 mg	95 % retention after 2000 cycles at 10 A g^{-1}	[15]
	Co_3O_4@NiAl-LDH	1800 F g^{-1}	3.9 mg	87.9 % retention after 2000 cycles at 8 A g^{-1}	[16]
	Ni-Co sulfide NWAs	~ 2500 F g^{-1}	2.5 mg	78.5 % retention after 3000 cycles at 15 A cm^{-2}	[17]
	NiO nanoarrays	2065 F g^{-1}	0.125 mg	88.9 % retention after 5000 cycles at 70 A g^{-1}	[18]
	Ni 2 P NS/NF	~ 3500 F g^{-1}	1.2 mg	72 % retention after 5000 cycles 10 A g^{-1}	[19]
Cu-coated polyimide film	**3D-NA/Ni/NiNPAs**	3264 F g^{-1} 979 mF cm^{-2}	0.3 mg	88 % retention after 20000 cycles at 100 mA cm^{-2}	This work
Flexible substrate	**$NiCo_2O_4$ with P123 and EG on carbon cloth**	~ 608 mF cm^{-2}	0.33 mg	90 % retention after 4000 cycles at 10 A g^{-1}	[20]
	graphite/Ni/Co_2NiO_4-CP on cellulose paper	600 mF cm^{-2}	1.55 mg	98 % retention after 15000 cycles	[21]
	Ni/Co-LDHs pressed on flexible Ni foam	~ 1000 mF cm^{-2}	0.5 - 0.8 mg	-	[22]
	NiO/$Ni(OH)_2$ nanoflowers encapsulated in 3,4-ethylenedioxythiophene	400 mF cm^{-2} at 4 mA cm^{-2}	-	82.2 % retention after 1000 cycles at 4 mA cm^{-2}	[23]

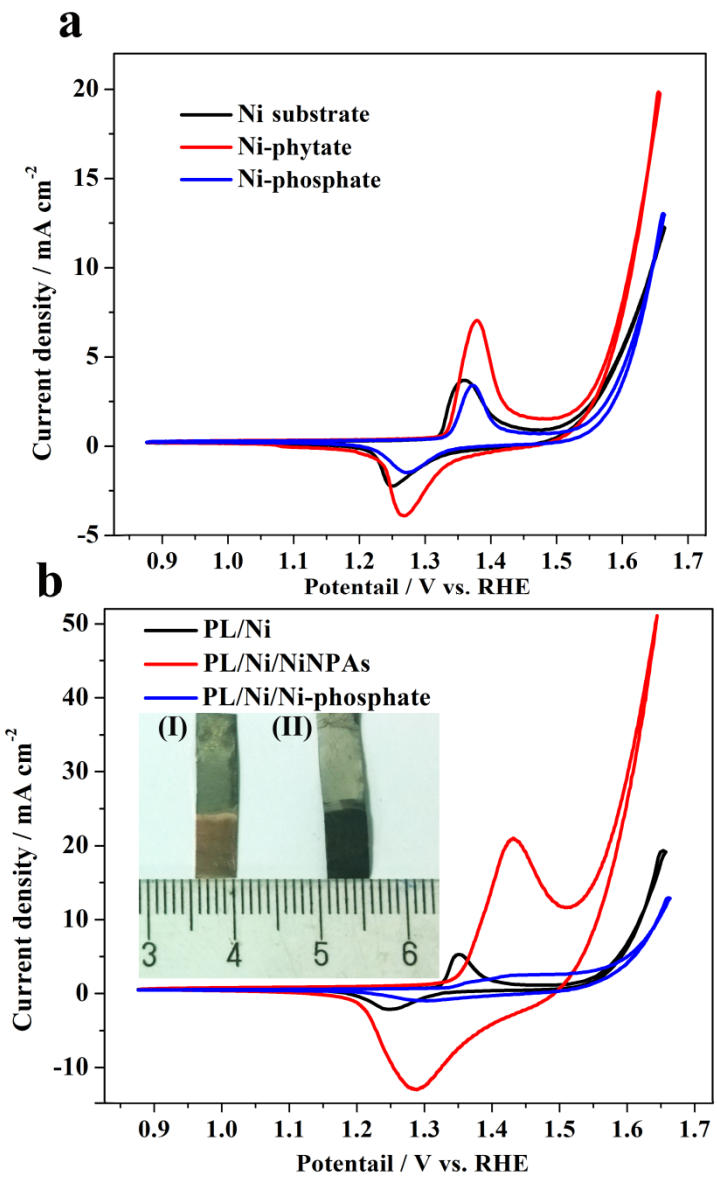

Fig. S12 CVs of commercial Ni foil (a) and PL/Ni (b) with the treatment of 1M phytic acid for 13h and 1M phosphoric acid for 3h, respectively. The inset of Fig.S11b shows the photographs of PL/Ni immersed in phosphoric acid (I) and phytic acid (II).

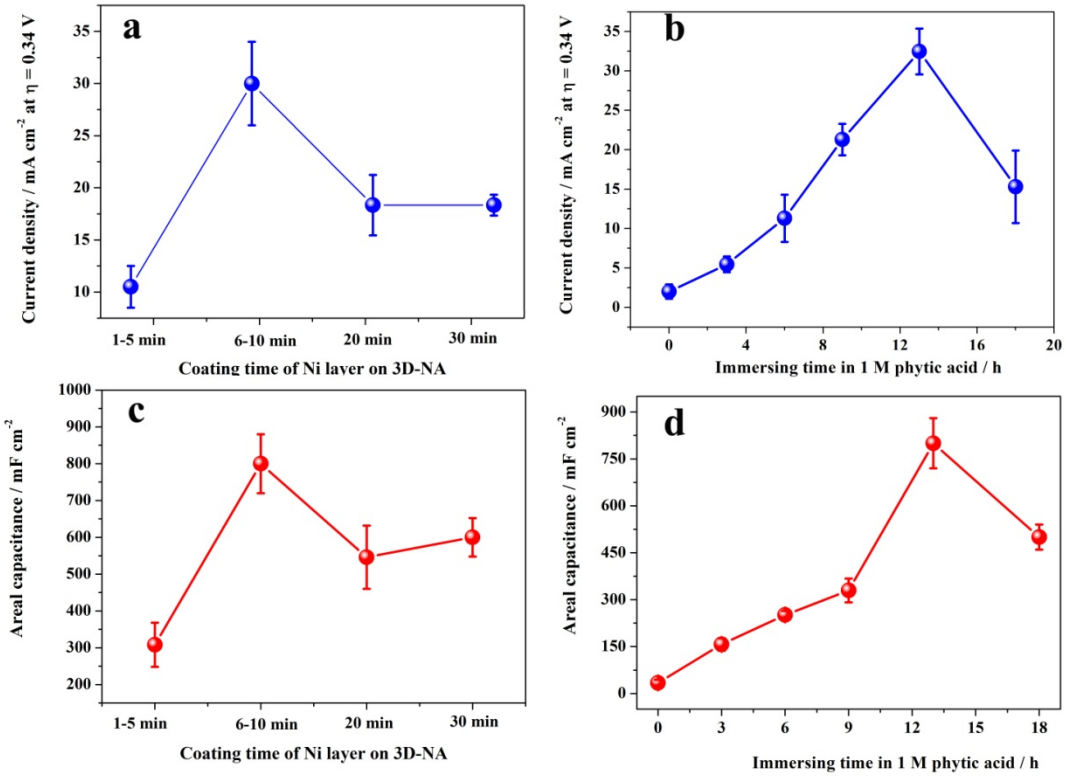

Fig. S13 The investigations of coating time of Ni plating and immersing time in 1 M phytic acid for OER activities (a-b) and capacitive performance (c-d).

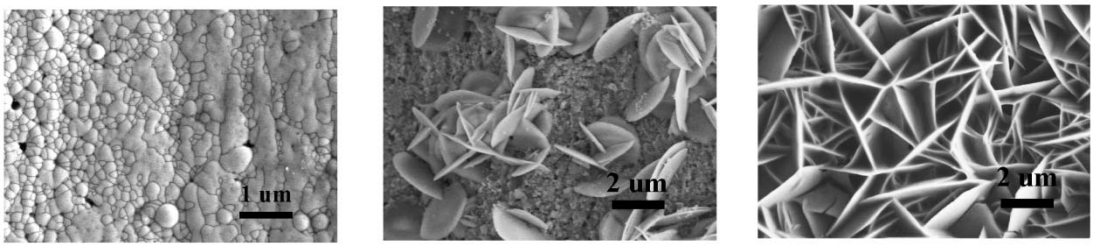

Fig. S14 SEM images of PL/Ni/NiNPAs (coating for 7 min) with different immersing time in 1 M phytic acid.

Table S6. The active nickel plating mass and active materials mass of each electrode at the fixed conditions.

Coating time investigation			**Immersing time investigation**	
Coating time (min)	**m_{Ni}* (mg cm^{-2})**	**m_a*(mg cm^{-2}, immersing for 13 h)**	**Immersing time (h)**	**m_a*(mg cm^{-2}, coating for 7 min)**
1-5 min	0.72	0.16	**3 h**	0.81
6-10 min	1.00	0.30	**6 h**	0.62
20 min	1.76	0.76	**9 h**	0.37
30 min	2.24	1.24	**13 h**	0.20
			18 h	0.09

*the mass per square centimeter is obtained by the weight difference between the substrate (3D-NA or PL) and the electrode at the fixed condition and the final values are generally the average of 5 individual electrodes.

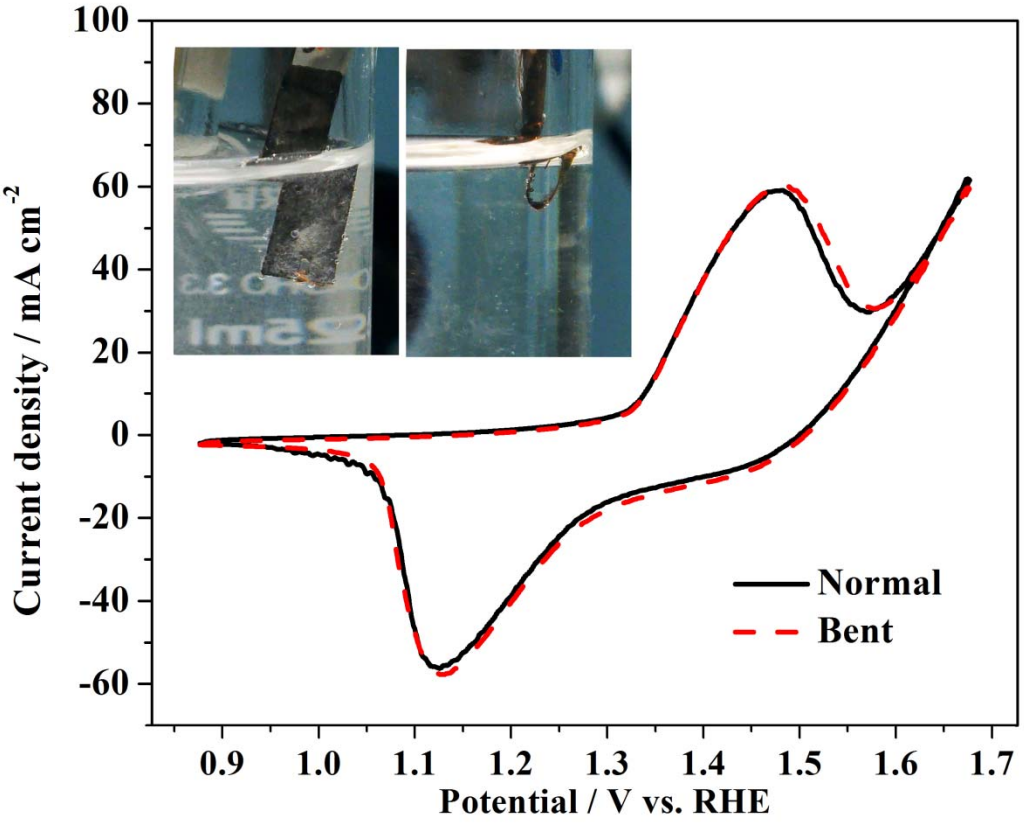

Fig. S15 CVs of 3D-NA/Ni/NiNPAs electrode at two different conditions and the inset is the optical images of the electrode at the normal and bending state.

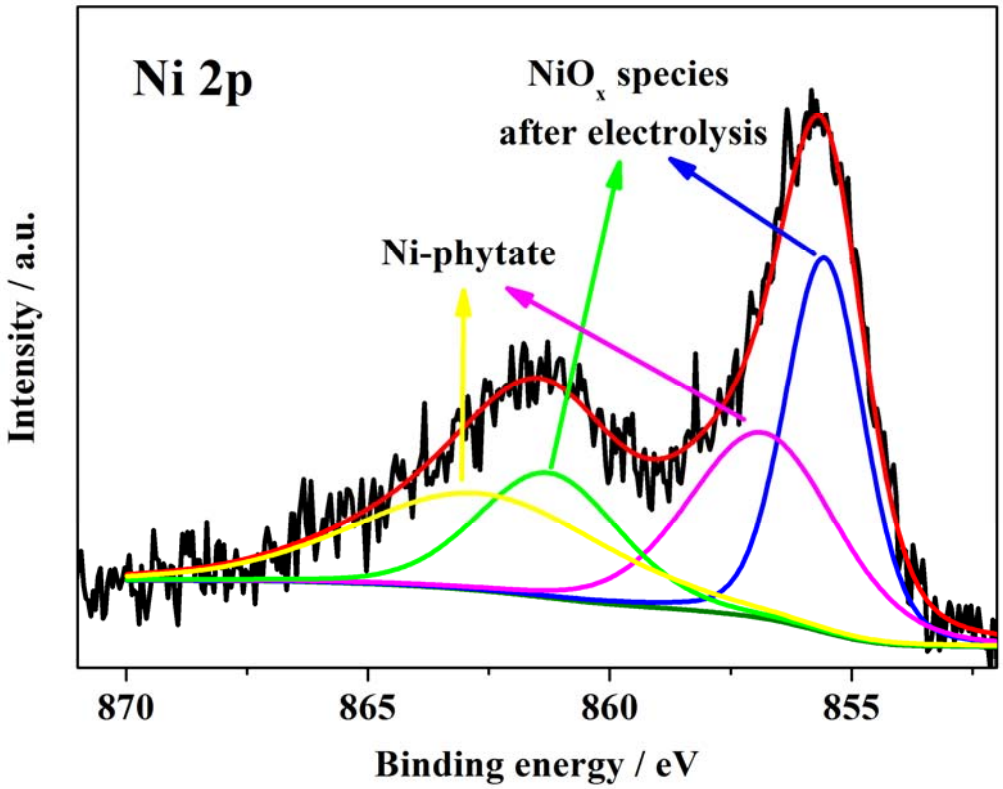

Fig. S16 Ni 2p spectrum of 3D-NA/Ni/NiNPAs after electrolysis.

Ni 2p spectrum of 3D-NA/Ni/NiNPAs after electrolysis has been deconvoluted into four peaks at 855.5 eV, 856.8 eV, 861.3 eV and 862.5 eV, assigned to NiO_x species and Ni-phytate, respectively. The proportion of converted Ni-phytate could be calculated to be approximate 48 % according to the integrated area of each portion.

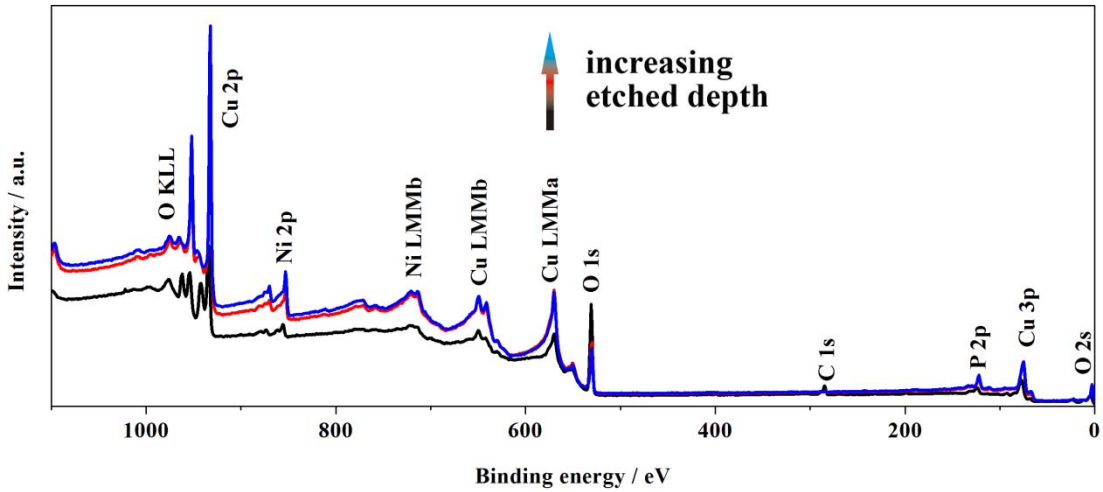

Fig. S17 The survey scan depth-profiling XPS spectra of 3D-Ni/Ni/NiNPAs electrode after electrolysis.

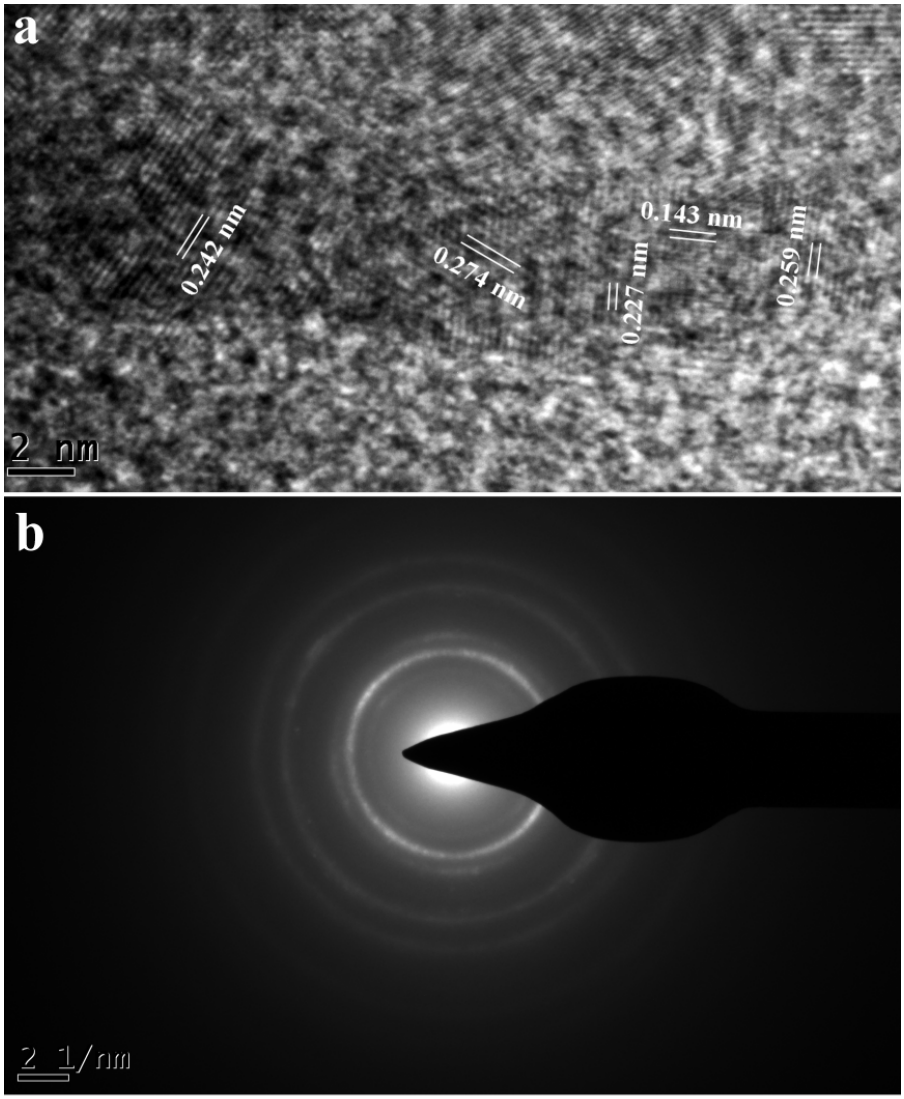

Fig. S18 (a) TEM and the lattice fringes spacing (marked in white) of the nanofibers; (b**)** the SAED pattern of Ni-phytate nanoplates after catalysis.

Reference:

[1] X. Zhang, H.M. Xu, X.X. Li, Y.Y. Li, T.B. Yang, Y.Y. Liang, Facile Synthesis of Nickel-Iron/Nanocarbon Hybrids as Advanced Electrocatalysts for Efficient Water Splitting. *ACS Catal.* **2016,** *6*, 580.

[2] X.M. Zhou, Z.M. Xia, Z.Y. Zhang, Y.Y. Ma, Y.Q. Qu, One-step synthesis of multi-walled carbon nanotubes/ultra-thin Ni(OH)(2) nanoplate composite as efficient catalysts for water oxidation. *J. Mater. Chem. A* **2014,** *2*, 11799.

[3] X.J. Cui, P.J. Ren, D.H. Deng, J. Deng, X.H. Bao, Single layer graphene encapsulating non-precious metals as high-performance electrocatalysts for water oxidation. *Energy Environ. Sci.* **2016,** *9*, 123.

[4] V. Augustyn, S. Therese, T.C. Turner, A. Manthiram, Nickel-rich layered LiNi1-xMxO2(M = Mn, Fe, and Co) electrocatalysts with high oxygen evolution reaction activity. *J. Mater. Chem. A* **2015,** *3*, 16604.

[5] M. Gao, W. Sheng, Z. Zhuang, Q. Fang, S. Gu, J. Jiang, Y. Yan, Efficient Water Oxidation Using

Nanostructured α-Nickel-Hydroxide as an Electrocatalyst. *J. Am. Chem. Soc.* **2014,** *136*, 7077.
[6] L.L. Feng, G.T. Yu, Y.Y. Wu, G.D. Li, H. Li, Y.H. Sun, T. Asefa, W. Chen, X.X. Zou, High-Index Faceted Ni3S2 Nanosheet Arrays as Highly Active and Ultrastable Electrocatalysts for Water Splitting. *J. Am. Chem. Soc.* **2015,** *137*, 14023.
[7] S.W. Li, Y.C. Wang, S.J. Peng, L.J. Zhang, A.M. Al-Enizi, H. Zhang, X.H. Sun, G.F. Zheng, Co-Ni-Based Nanotubes/Nanosheets as Efficient Water Splitting Electrocatalysts. *Advanced Energy Materials* **2016,** *6*.
[8] H.F. Liang, F. Meng, M. Caban-Acevedo, L.S. Li, A. Forticaux, L.C. Xiu, Z.C. Wang, S. Jin, Hydrothermal Continuous Flow Synthesis and Exfoliation of NiCo Layered Double Hydroxide Nanosheets for Enhanced Oxygen Evolution Catalysis. *Nano Lett.* **2015,** *15*, 1421.
[9] S. Chen, J.J. Duan, J.R. Ran, M. Jaroniec, S.Z. Qiao, N-doped graphene film-confined nickel nanoparticles as a highly efficient three-dimensional oxygen evolution electrocatalyst. *Energy Environ. Sci.* **2013,** *6*, 3693.
[10] H.Y. Wang, Y.Y. Hsu, R. Chen, T.S. Chan, H.M. Chen, B. Liu, Ni3+-Induced Formation of Active NiOOH on the Spinel Ni-Co Oxide Surface for Efficient Oxygen Evolution Reaction. *Advanced Energy Materials* **2015,** *5*.
[11] Z. Peng, D.S. Jia, A.M. Al-Enizi, A.A. Elzatahry, G.F. Zheng, From Water Oxidation to Reduction: Homologous Ni-Co Based Nanowires as Complementary Water Splitting Electrocatalysts. *Advanced Energy Materials* **2015,** *5*.
[12] L. Kuai, J. Geng, C. Chen, E. Kan, Y. Liu, Q. Wang, B. Geng, A Reliable Aerosol-Spray-Assisted Approach to Produce and Optimize Amorphous Metal Oxide Catalysts for Electrochemical Water Splitting. *Angew. Chem. Int. Ed.* **2014,** *53*, 7547.
[13] F. Song, X.L. Hu, Exfoliation of layered double hydroxides for enhanced oxygen evolution catalysis. *Nature Communications* **2014,** *5*.
[14] L.A. Stern, L.G. Feng, F. Song, X.L. Hu, Ni2P as a Janus catalyst for water splitting: the oxygen evolution activity of Ni2P nanoparticles. *Energy Environ. Sci.* **2015,** *8*, 2347.
[15] X. Ma, Y. Li, Z. Wen, F. Gao, C. Liang, R. Che, Ultrathin β-Ni(OH)2 Nanoplates Vertically Grown on Nickel-Coated Carbon Nanotubes as High-Performance Pseudocapacitor Electrode Materials. *ACS Appl. Mat. Interfaces* **2015,** *7*, 974.
[16] F. Ning, M. Shao, C. Zhang, S. Xu, M. Wei, X. Duan, Co3O4@layered double hydroxide core/shell hierarchical nanowire arrays for enhanced supercapacitance performance. *Nano Energy* **2014,** *7*, 134.
[17] Y. Li, L. Cao, L. Qiao, M. Zhou, Y. Yang, P. Xiao, Y. Zhang, Ni-Co sulfide nanowires on nickel foam with ultrahigh capacitance for asymmetric supercapacitors. *J. Mater. Chem. A* **2014,** *2*, 6540.
[18] V. Senthilkumar, F.B. Kadumudi, N.T. Ho, J.W. Kim, S. Park, J.S. Bae, W.M. Choi, S. Cho, Y.S. Kim, NiO nanoarrays of a few atoms thickness on 3D nickel network for enhanced pseudocapacitive electrode applications. *J. Power Sources* **2016,** *303*, 363.
[19] K. Zhou, W. Zhou, L. Yang, J. Lu, S. Cheng, W. Mai, Z. Tang, L. Li, S. Chen, Ultrahigh-Performance Pseudocapacitor Electrodes Based on Transition Metal Phosphide Nanosheets Array via Phosphorization: A General and Effective Approach. *Adv. Funct. Mater.* **2015,** *25*, 7530.
[20] S. Gao, F. Liao, S. Ma, L. Zhu, M. Shao, Network-like mesoporous NiCo2O4 grown on carbon cloth for high-performance pseudocapacitors. *J. Mater. Chem. A* **2015,** *3*, 16520.
[21] J.X. Feng, S.H. Ye, A.L. Wang, X.F. Lu, Y.X. Tong, G.R. Li, Flexible Cellulose Paper-based Asymmetrical Thin Film Supercapacitors with High-Performance for Electrochemical Energy Storage. *Adv. Funct. Mater.* **2014,** *24*, 7093.

[22] T. Li, G.H. Li, L.H. Li, L. Liu, Y. Xu, H.Y. Ding, T. Zhang, Large-Scale Self-Assembly of 3D Flower-like Hierarchical Ni/Co-LDHs Microspheres for High-Performance Flexible Asymmetric Supercapacitors. *ACS Appl. Mat. Interfaces* **2016,** *8*, 2562.
[23] H.L. Yang, H.H. Xu, M. Li, L. Zhang, Y.H. Huang, X.L. Hu, Assembly of NiO/Ni(OH)(2)/PEDOT Nanocomposites on Contra Wires for Fiber-Shaped Flexible Asymmetric Supercapacitors. *ACS Appl. Mat. Interfaces* **2016,** *8*, 1774.